HHS Public Access

Author manuscript

Nat Neurosci. Author manuscript; available in PMC 2011 July 20.

Published in final edited form as:

Nat Neurosci. 2010 November ; 13(11): 1413–1420. doi:10.1038/nn.2659.

The functional asymmetry of auditory cortex is reflected in the organization of local cortical circuits

Hysell V. Oviedo[1], **Ingrid Bureau**[2], **Karel Svoboda**[3], and **Anthony M. Zador**[1]

[1]Cold Spring Harbor Laboratory, 1 Bungtown Road, Cold Spring Harbor, NY 11724, USA

[2]INSERM, U901, INMED, Marseille 13273, France

[3]Janelia Farm Research Campus, Howard Hughes Medical Institute, Ashburn, VA 20147, USA

Abstract

The primary auditory cortex (A1) is organized tonotopically, with neurons sensitive to high and low frequencies arranged in a rostro-caudal gradient. We used laser scanning photostimulation in acute slices to study the organization of local excitatory connections onto layers 2 and 3 (L2/3) of the mouse A1. Consistent with the organization of other cortical regions, synaptic inputs along the isofrequency axis (orthogonal to the tonotopic axis) arose predominantly within a column. Surprisingly, we found that local connections along the tonotopic axis differed from those along the isofrequency axis: some input pathways to L3 (but not L2) arose predominantly out-of-column. In vivo cell-attached recordings revealed differences between the sound-responsiveness of neurons in L2 and L3. Our results are consistent with the hypothesis that auditory cortical microcircuitry is specialized to the unique one-dimensional representation of frequency in the auditory cortex.

A widespread and appealing hypothesis is that all cortical areas (e.g. visual and auditory) are wired according to the same general schema, regardless of what computation is performed in each area. According to this canonical model of cortical circuitry [1], information from the thalamus enters the cortex via thalamocortical synapses onto neurons in cortical layer 4 (L4), and these L4 neurons then transmit information to neurons in L2/3 and then to layer 5 (L5) (e.g. refs. [2, 3]). This canonical circuit model represents the synthesis of several decades of careful neuroanatomy and neurophysiology probing the circuitry of visual cortex, the first area in which microcircuitry was examined in detail.

The introduction of laser scanning photostimulation (LSPS) has made it possible to examine the microcircuitry in other cortical areas with high efficiency. LSPS uses the photorelease of caged glutamate to map functional connections between a neuron and its presynaptic inputs *in vitro* (refs. [4, 5]). This technique has revealed distinct patterns of functional connectivity in different cortical areas, including the barrel (refs. [3, 6]), motor [7] and auditory [8] cortices. These

Contributions

H.V.O. and A.M.Z. conceived the experiments, analyzed the data and wrote the paper.

H.V.O. performed all the experiments. I.B. and K.S. provided expert advice and LSPS experimental set-up.

studies showed that although in broad strokes the canonical model of visual cortex may be valid in non-visual cortical areas, there are also important area-specific differences in local circuitry. Thus each cortical area may represent a variation on the canonical circuit, specialized for the implementation of the cortical computation that occurs within that area.

In the primary auditory cortex of all species studied to date, there is a characteristic map reflecting the tonotopic organization of sound frequency in the cochlea. In the mouse, as in many other species, high frequencies are represented in the rostral part of the cortex and low frequencies in the caudal [9]. This one-dimensional tonotopic axis can be considered the analogue of two-dimensional space in the visual and somatosensory cortices, in that it reflects directly the organization of sensory receptors at the periphery. However, because the representation of sound frequency along the cochlea is intrinsically one-dimensional, the organization of auditory cortex along the axis orthogonal to the tonotopic cortical axis cannot immediately be inferred from the organization of the sensory periphery (but see [10]). The auditory cortex is thus functionally anisotropic: the functional organization along the tonotopic axis is qualitatively different from the organization orthogonal to the tonotopic axis. In this respect the auditory cortex differs from both the visual and somatosensory cortices, where the two-dimensional organization of the sensory periphery is reflected directly in the organization of the corresponding cortex. What is not known is how this functional anisotropy—i.e. the spatial arrangement of tuned neurons—is reflected at the microcircuit level.

To determine how the functional anisotropy of auditory cortex observed *in vivo* is reflected in the local microcircuitry probed *in vitro*, we have used LSPS to compare the organization of mouse primary auditory cortex slices cut along the tonotopic axis with those cut perpendicular to that axis. Here we report that local inputs to L2/3 differ depending on whether or not the slice is cut to preserve information across frequencies. Furthermore, *in vivo* cell-attached recordings revealed differences between the sound-responsiveness of neurons in L2 and L3. Our results are consistent with the hypothesis that auditory cortical microcircuitry is specialized to the unique one-dimensional representation of frequency in the auditory cortex.

Results

We first investigated the organization of synaptic inputs to L2/3 of mouse primary auditory cortex in a coronal slice cut to preserve isofrequency bands (“isofrequency slices”). We next examined the organization of inputs to L2/3 in a horizontal slice, which allowed us to probe organization across different frequencies (“tonotopic slices”). Finally, we performed *in vivo* cell-attached recordings targeted at L2/3 neurons to explore whether the differences in local circuitry we observed *in vitro* lead to functional differences in stimulus-driven responses *in vivo*.

Organization of synaptic inputs into L2/3 along the isofrequency axis

We began by studying the input to neurons in L2/3 in a coronal slice that preserves isofrequency bands (Fig. 1a, top), *i.e.* in a slice containing neurons which respond to similar frequencies [9]. The organization of the primary auditory cortex along this axis has recently

been characterized in the rat [8], but to assess any species-specific differences in input pattern (as has been shown in the barrel cortex [6] for example), and to provide a baseline for the studies presented here, we repeated these experiments in the mouse.

We performed whole-cell recordings from excitatory neurons (n = 26) in L2/3. We isolated excitatory postsynaptic currents (EPSCs) by voltage-clamping near the inhibitory reversal potential (−70 mV). To characterize synaptic inputs, we added caged glutamate to the fluid bathing the slice and photoreleased at the focal spot of an ultraviolet (UV) laser beam (see Methods, Fig. 1b left). Photorelease of caged glutamate near the patched neuron evoked a large short-latency *direct response* (Fig. 1c, left), mediated mainly by glutamate receptors near or on the soma, of sufficient magnitude to trigger one or a few action potentials under current clamp conditions. Photorelease of caged glutamate at other locations in the slice elicited either *no response*, or a *synaptic response* (Fig. 1c, right). The synaptic responses, which are the focus of this study, result from action potentials in presynaptic neurons whose axons connect to the neuron from which we are recording. Direct responses can be distinguished from synaptic responses by their larger amplitudes (note difference in scale between Fig. 1c left and right) and shorter latency (see Methods).

To facilitate comparison across experiments, we aligned the UV stimulation grid for all cells consistently, using landmarks in the slice (Fig. 1a, bottom; see Methods for details). To minimize differences arising from slice-to-slice variability in the alignment along the x-axis of the grid with the landmarks, we present average population maps with all the somata aligned to the center of the map. We filled each neuron with a fluorescent marker (Alexa-594) to confirm that the dendritic tree was mostly contained within the slice, and to establish whether spines were present (Fig. 1b, right). All cells analyzed in this study were excitatory, based on morphology and the presence of spines.

Representative synaptic input maps for neurons in L2 and L3 in isofrequency slices are shown in Fig. 2a-b, respectively. (See Supplementary Fig. 1 for all input maps analyzed). The pattern of input into L2/3 largely followed the columnar organization of the canonical cortical circuit. Averaging across slices (Fig. 2c), we found that the L2/3 intralaminar connections provided the largest source of input, followed by L4 and L5, with only a small contribution from layer 6 (L6) (Fig. 2d, left).

To examine specific differences between inputs to L2 and L3 we examined the average input to each layer separately (Fig. 2d, right). Neurons in L2 and L3 were readily distinguished based on previously described laminar boundaries [11], and our own experimental observations that: (1) L2 appears as the densest cortical layer under infrared gradient contrast optics (average thickness of 100 μm; see Fig. 3a); and (2) there are significant morphological differences between neurons in L2 and L3 (see Fig. 6a–b for examples and ref. [6]). Layer 2 neurons had a non-classic pyramidal shape with their apical dendrites branching close to the cell body, whereas L3 neurons had a classic pyramidal shape. Quantitative comparison of the inputs to L2 (n = 11 neurons) and L3 (n = 15 neurons) revealed largely similar inputs into both layers, with the exception of significant input from deep layers into L2 but not L3 (Fig. 2d, right). This input arose from the border of L5/6 and was not observed in the rat auditory cortex[8]. Layer 3 had strong recurrent connections that

are also largely absent in the rat. However, given the extensive lemniscal thalamocortical projections in L3 of the mouse [12], the prominent L3 to L3 connections we observe in the mouse may not represent a significant deviation from the classic L4 to L3 pathway.

Asymmetric organization of synaptic inputs into L2/3 along the tonotopic axis

The laminar and columnar organization of synaptic inputs into L2/3 described so far were observed in a slice preparation that did not preserve the tonotopic map of the auditory cortex. To examine the organization of synaptic inputs into L2/3 across the tonotopic axis (oriented anterior to posterior [9, 13, 14]) we conducted a new series of experiments using horizontal slices (Fig. 3a). These slices were prepared in the same orientation as the auditory thalamocortical slice preparation developed to optimize the input from the ventral division of the medial geniculate nucleus (MGBv) of the thalamus to A1 [12]. We used the rostral tip of the hippocampus to align the stimulus grid along the x-axis (Fig. 3a, bottom).

To confirm that our cortical recordings were indeed in A1, we performed two sets of control experiments using thalamocortical slices. First, we confirmed physiologically with thalamic LSPS experiments that there were direct synaptic inputs into layers 3 and 4 of the cortical area in which we performed all our subsequent cortical mapping experiments (Supplementary Fig. 2). Second, to confirm the anatomy we made small injections of the retrograde tracer DiI into the putative A1 cortical area mapped (Supplementary Fig. 3). In all cases (n = 6) we found fibers labeled only in the MGBv, consistent with previous results [12]. These experiments confirmed that the cortical area mapped in horizontal slices was located within A1.

We investigated the functional organization of synaptic inputs within A1 across the tonotopic axis by recording from L2/3 excitatory cells (n = 48). We analyzed separately the inputs to neurons in L2/3 in tonotopic slices. Inputs to L2 (n = 15) in these slices showed a pattern similar to that found in L2 of the isofrequency slices. There was strong input from the border of L5/6 and local connections (Fig. 3b, top and middle). Thus the pattern of connectivity to L2 was the same along the tonotopic axis as across it.

Surprisingly, the pattern of inputs to L3 neurons (n = 15) in tonotopic slices differed from the pattern of inputs in isofrequency slices. Along the tonotopic axis L6 input, which was largely absent in the isofrequency slices, emerged as an important source of input (Fig. 3c and e). Moreover, the L6 input was spatially shifted along the horizontal axis (Fig. 3c, middle): the L6 input did not arise mainly from within-column neurons located directly below the recorded neurons, but rather from more anterior sites of the primary auditory cortex, presumably corresponding to neurons tuned to higher frequencies.

To test whether this shift was somehow specific to the particular site from which we chose to record, we also recorded from pairs of L2/3 neurons separated by 250–300μm in the same slice. We found that the connectivity was invariant to this translation along the tonotopic axis (Supplementary Fig. 4). We therefore grouped the data from both clusters for further analysis. (See Supplementary Figs. 5 and 6 for all input maps analyzed for tonotopic slices). The average population map for L2 confirmed columnar input organization (Fig. 3b,

bottom), and for L3 out-of-column L5/6 input (Fig. 3c, bottom) coupled with strong intralaminar input (Fig. 3d).

We characterized the asymmetry of input to L3 with several analyses. First, to quantify the horizontal shift on a cell-by-cell basis, we computed the horizontal distance between the soma of the recorded neuron and its deep L5 and L6 hotspot (d_{s-h}, see Methods for details). This analysis revealed a clear horizontal shift in the input to L3 (but not L2) in tonotopic slices, but none along the isofrequency axis (Fig. 4a–b, top). Unlike L2 neurons which received mainly columnar input, L3 cells received horizontally shifted inputs from as far as 400 μm away from the soma ($P << 0.01$, n = 39, t-test). Second, we calculated the average input arising from deep L5 and L6 from the average population maps (Fig. 4a–b, bottom). Consistent with the previous analysis of hotspots, this analysis revealed that inputs from deep L5 and L6 to L3 were shifted anteriorly with respect to L2 in tonotopic (Fig. 4a, bottom) but not isofrequency (Fig. 4b, bottom) slices. Because there is an anterior-posterior map of frequency in the primary auditory cortex, our results suggest that the input to L3 arises from out-of-column neurons in L6 tuned to higher frequencies.

Laminar input analysis showed that L3 contributed significantly more input to itself than to L2 in tonotopic slices (Fig. 3d). To determine whether this relative increase in L3 intralaminar input was due to an asymmetry in the connectivity within L3, we compared the intralaminar input within L3 (i.e. the L3 to L3 input) arising from the higher frequency side to that arising from the lower frequency side. We found that the average L3 input from the higher frequency side was significantly stronger than from the lower frequency side in the tonotopic slices (Fig. 4c, left, $P < 0.05$, n = 23, t-test), but no such intralaminar input asymmetry was found in the isofrequency slices (Fig. 4c, right, $P = 0.85$, n = 15, t-test). Thus in addition to the bias in high frequency inputs from L6, there was also a tendency for local recurrent connections to arise from L3 neurons positioned at higher frequencies along the tonotopic axis. Taken together, these columnar and laminar differences of synaptic input into L3 across axes of stimulus representation suggest that L3 neurons receive disproportionately more input from neurons tuned to higher frequencies.

Shared input among nearby neurons

LSPS scanning showed that neurons in L2/3 received a large proportion of their input from nearby neurons in the same layer. Along the tonotopic axis, L2 and L3 received 45% of their input from local L2/3 connections (Fig. 3d). Along the isofrequency axis the proportion of local input was even higher; L2 received 54% and L3 60% from local L2/3 connections (Fig. 2d, right). The contribution of intralaminar input to L2/3 in auditory cortex was higher than comparable values estimated using LSPS in visual (26% [2]) and barrel (36% for L2 and 19% for L3 [6]) cortices. These values probably represent an underestimate of the contribution of local inputs, because with LSPS very local (< 100 μm) input is mixed with direct responses and thus are not included (see e.g. ref. [15]).

Given that nearby neurons are highly interconnected, we wondered about the extent to which nearby neurons received similar input. If the pattern of synaptic inputs to nearby neurons were very similar, this would support the idea that nearby neurons are performing similar—perhaps redundant—computations. To assess the similarity of inputs, we compared

synaptic maps recorded from two or more neurons within a single slice. We quantified similarity by computing the correlation between pairs of average maps. A correlation of unity implies that the input maps of two neurons are identical, whereas a correlation of zero implies that the input to two neurons is independent. In practice, the maximum observable correlation is limited by noise, which can be estimated by computing the correlation of maps from a single neuron to itself. This procedure provides an average upper bound of approximately 0.75, similar to that reported in the barrel cortex [3].

The pairwise map correlation as a function of intersomatic distance is shown in Fig 5. For both tonotopic and isofrequency slices, the correlation was largest for neurons closest together and declined with distance. The mean correlation between the nearest (< 100 μm) pairs was 0.30±0.02 and 0.34±0.04 for the tonotopic and isofrequency slices (respectively), and was lower than that between more distant (>100 μm) pairs (0.2±0.04 and 0.18±0.04 for the tonotopic and isofrequency slices.) To quantify the decrease in correlation with distance, we fitted the data with a simple exponential $c = 0.37 * exp(-x/159)$, where x is the intersomatic distance (in micrometers). Thus nearby neurons are not very correlated, and the correlation falls off rapidly, with a decay of about 159 μm.

Differences in response properties and projections between L2 and L3

The differences we observed between L2 and L3 input patterns *in vitro* suggested that neurons in these layers might have functionally distinct responses to sounds. To test this hypothesis, we used *in vivo* cell-attached methods [16] to compare tuning curves (100 and 500 milliseconds pure tones, five octaves, four intensities) of neurons in L2/3. After each recording, we electroporated each neuron with biocytin for later histological analysis (refs. [17, 18]). We recovered the morphology of 20 presumed excitatory neurons (based on the presence of spines) with either a non-classic pyramidal shape (n = 10, found exclusively in L2, similar to mouse barrel cortex [6]; Fig. 6a, left) or classic pyramidal neurons (n = 10, found in L3, Fig. 6b, right). Based on their anatomical position, all cells recovered were within primary auditory cortex (Fig. 6d).

Tuning curves in L2 and L3 were clearly different (Fig. 6a–b). Pure tones significantly increased the firing rate of L2 cells above background compared to L3 (Fig. 6c). L2 neurons were more responsive, and tended to be tuned to stimulus frequency in an intensity-dependent manner: tuning width (*i.e.* the range of frequencies which elicited a response) increased with tone intensity (Fig. 6a, right). We did not recover any L3 neurons with clear frequency tuning; most showed little or no tone-evoked response (Fig. 6b, left). Responses to other stimuli such as white noise were also different (Supplementary Fig. 7).

Finally, we examined whether L2 and L3 also differed in their long-range projections. To test for differences, we chose the interhemispheric pathway between the auditory cortices. We injected the retrograde tracer cholera toxin in the right auditory cortex to reveal projections arising from the left auditory cortex (the hemisphere characterized in this study). The laminar pattern of interhemispheric projections revealed another difference between L2 and L3: Layer 3 projects to the contralateral auditory cortex, whereas L2 does not (Fig. 6e, 4/4 animals). Thus the differences in local circuitry between L2 and L3 along the tonotopic axis are associated with differences in both long-range connectivity and sound-evoked

responses *in vivo*, suggesting that these neuronal populations may be play different functional roles.

Discussion

We have used LSPS to study the local inputs to L2 and L3 in auditory cortex. Our main findings are that (1) the local input to L3 is anisotropic (i.e. it is different along and across the tonotopic axis), with out-of-column input to L3 arising preferentially from higher frequencies, particularly from L3 and L6; (2) nearby neurons share only modest input, and the amount of shared input decreases rapidly (space constant λ = 159 μm); and (3) these differences in local circuitry are associated with functional differences in sound responsiveness.

Anisotropy of columnar structure in auditory cortex

The map of acoustic space in the auditory cortex is functionally anisotropic: there is a low-to-high frequency organization of neurons along the tonotopic axis that is absent along the orthogonal isofrequency axis. Our most surprising finding was that this anisotropy was reflected in the local circuitry of inputs to L3, manifested as a difference between the local circuitry preserved within tonotopic and isofrequency slices (Figs. 2 and 3). Specifically, in tonotopic slices, L3 neurons preferentially received inputs from out-of-column neurons in L6. Furthermore, the input from L6 was asymmetric, arising preferentially from anterior parts of the auditory cortex corresponding to regions of the tonotopic map tuned to higher frequencies. This anisotropy in connectivity was not a general property of horizontal slices (*e.g.* it was not present in nearby somatosensory areas; Supplementary Fig. 8), but appears to be a specific reflection of the uniquely anisotropic auditory cortical map.

The high-frequency bias in tonotopic slices was most marked in L3 inputs from L6 and L3. The lateral distance of these shifted L6 inputs ranged from 200 to 400 μm (Fig. 4a). Given the size of the mouse auditory cortex (just over 1 mm along the horizontal plane covering 6 octaves [9]), the L3 cells receiving spectrally shifted input from L6 neurons could be integrating across at least 1 to 3 octaves. The bias in the high frequency L3 to L3 input was comparably large.

Anisotropic organization along the tonotopic axis is not unique to the mouse. Differences in the connectivity between the tonotopic and isofrequency axes have previously been reported in both the rabbit [19] and the cat [20]. Although anisotropic organization was not previously reported in a study of coronal (isofrequency) rat primary auditory cortex slices [8], we observed clear evidence of anisotropy in horizontal (tonotopic) slices (Supplementary Fig. 9). This anisotropic organization may thus be a universal feature of auditory cortex across species.

L2 and L3 are distinct in auditory cortex

In many areas of cortex, no distinction is made between layers 2 and 3: L2/3 is treated as a single homogenous functional unit. Our results, however, indicated that in the auditory cortex, neurons in these two laminae were distinct with respect to morphology, connectivity, and function. Morphologically, L2 and L3 pyramidal cells differed (Fig. 6; see also ref. [6]):

L3 neurons had a classic pyramidal shape, whereas L2 cells lacked an elongated apical shaft and instead had dendrites that arborized parallel to the slice. At the level of local connectivity, the pattern of intracortical synaptic input was also distinct between these layers, especially along the tonotopic axis: L2 received columnar input whereas L3 received out-of-column input (Fig. 3b and c, Fig. 4a). We also found that neurons in L3 but not in L2 project to the contralateral cortex, similar to the pattern observed in the auditory cortex of the cat and rat (Fig. 6e; refs. [21–23]).

Finally, neurons in the two layers differed functionally with respect to their responsiveness to simple auditory stimuli such as pure tones and white noise. Layer 2 cells were more responsive and showed well-defined frequency tuning to pure tones, whereas L3 cells were largely unresponsive (Fig. 6). This difference in responsiveness is consistent with recent results using photostimulation-assisted identification of neuronal populations (PINP) showing that contralaterally projecting L3 neurons (functionally tagged with channelrhodopsin-2) are not responsive to simple auditory stimuli [23]. These observations suggest that L2 and L3 may play distinct functional roles.

Although L2 and L3 appear to be functionally distinct in A1, the anatomical and functional boundary between L3 and L4 is less clear in A1 compared to other sensory cortices. Layer 4 in A1 lacks the characteristic spiny stellate cells found in other sensory regions [24], and sends projections to contralateral A1 (Fig 6e and ref. [22]). Layer 3 and L4 in A1 are quite similar in several other respects: both layers receive equally strong thalamic input (as measured by current source density [12]), and show equally strong cytochrome oxidase staining in the mouse [11], a feature that is classically used to identify L4 in other regions.

Weak local connectivity in auditory cortex

To what extent do nearby neurons in the cortex form a functional unit? In the primary visual cortex of cats and primates, neurons are functionally organized into orientation columns, defined by their shared preference for a particular visual orientation [25]. Columnar organization has since been described in many other cortical areas. A powerful form of columnar organization is found in the rodent whisker system [26], in which neurons within a cortical barrel encode activity of a single whisker and show strong local interconnectivity.

Strong columnar organization is not, however, universal across species and cortical areas. For example, the rodent visual cortex is not organized into orientation columns [27–29], as predicted by theoretical considerations of wire length [30]. These differences in the extent of columnar organization, as measured by the similarity of sensory responsiveness of nearby neurons *in vivo*, are reflected in the local organization of connections *in vitro*. For example, unconnected nearby neurons in L2/3 of the rat visual cortex share little excitatory input from lower layers, consistent with a model in which there are two or more interdigitated "subnetworks" [31].

Although there is some degree of gross tonotopy in the rodent auditory cortex, neurons do not appear to be organized into functional columns: nearby neurons can respond quite differently to the same stimulus (refs. [32–34]). These differences in response properties reflect an increase in coding independence from the inferior colliculus [35]. Consistent with this *in*

vivo organization, we found that the synaptic inputs to nearby neurons in L2 and L3 were quite different *in vitro*. Even for neurons closer than 100 μm, the pair-wise correlation of their input maps was 0.3, more than two-fold lower than observed in the rat within a barrel —consistent with the much stronger columnar organization within barrels—and comparable to that observed in the septa (*i.e.* the region between barrels [3]). Thus the weak tonotopic spatial organization found *in vivo* appears to be reflected in weak local connectivity.

Functional implications

Our main finding was that the organization of inputs onto L3 in primary auditory cortex was different along and orthogonal to the tonotopic axis. Although this anisotropy is, as far as is known, unique to the auditory cortex, it is consistent with the general principle that the organization of sensory maps reflects the statistics of sensory inputs. Just as the maps of space in the visual and barrel cortices mirror the organization of inputs at the retina and whiskers, respectively, the anisotropic organization of the auditory cortex reflects the one-dimensional organization of the cochlea.

Perhaps the most surprising observation was that the local circuits within A1 were not only anisotropic, but also asymmetric. In the tonotopic axis these connections could arise up to 400 μm away from the L3 neurons we mapped (Fig. 4a), consistent with integration over at least 3 octaves [9]. Our data suggest that the L6 to L3 pathway may also serve to relay spectrally distant input from up to 400 μm away. Interestingly, the intralaminar and L6 pathways were not mutually exclusive; we routinely found L3 neurons that received input from both (Supplementary Figs. 5 and 6).

Neural circuits in A1 are involved in the processing of spectrally complex sounds, including vocalizations, which requires integration over many frequencies [36–38]. Our data support a model for auditory cortex [39, 40], developed in part by analogy with the visual system ([41, 42]), in which intralaminar horizontal connections within L3 mediate this spectral integration. In addition, our data suggest that an out-of-column L6 pathway, possibly unique to auditory cortex, may also contribute to this spectral integration. By combining LSPS and other *in vitro* approaches with new optogenetic [23, 43], imaging [32, 33] and other technologies, we are now positioned to understand how *in vivo* sound responsiveness arises from the underlying circuitry of the auditory cortex.

Methods

Slice preparation and electrophysiology

Experiments used C57Bl6 and CBA mice and Long Evans rats in accordance with institutional animal care guidelines. We used young and adult mice from postnatal day 20 to 60 and juvenile rats (postnatal day 25–30). Animals were anesthetized and decapitated and the brains were transferred to a chilled cutting solution composed of (in mM): 110 choline chloride, 25 $NaHCO_3$, 25 D-glucose, 11.6 sodium ascorbate, 7 $MgCl_2$, 3.1 sodium pyruvate, 2.5 KCl, 1.25 NaH_2PO_4, and 0.5 $CaCl_2$. To examine synaptic connectivity along the tonotopic axis, we made horizontal slices with a 15-degree angle between the blade and the medial-lateral axis to obtain apical dendrites parallel to the slice and preserve

thalamocortical axons [12]. To examine synaptic connectivity along the isofrequency axis, we made coronal slices. All slices were 300 μm thick and were transferred to artificial cerebrospinal fluid (ACSF) containing (in mM): 127 NaCl, 25 $NaHCO_3$, 25 D-glucose, 2.5 KCl, 1 $MgCl_2$, 2 $CaCl_2$, and 1.25 NaH_2PO_4, aerated with 95% O_2 5% CO_2. The slices were incubated at 34° for 20–30 minutes and then kept at room temperature during the experiments. We also examined thalamocortical connectivity using the auditory thalamocortical slice in the mouse (500 μm thick [12])

Excitatory neurons 45–80 μm below the surface of the slice were visualized using infrared gradient contrast optics and patched with electrodes (6–7 MΩ) containing the following intracellular solution (in mM) 128 K-methylsulfate, 4 $MgCl_2$, 10 HEPES, 1 EGTA, 4 Na_2ATP, 0.4 Na_2GTP, 10 Na-phosphocreatine, and 0.015 Alexa-594 (Molecular Probes, Eugene, Oregon, USA); (pH 7.25); 300 mOsm. The presence of Alexa-594 in the internal solution rendered cells fluorescent. We confirmed that cells were excitatory by visualizing their dendritic arbor and spines. Filling each recorded cell with a fluorescent marker also gave us a way to reliably measure the angle between the slice and the neuronal processes to get immediate confirmation that in both horizontal and coronal slices the main arborizations were intact. Whole-cell recordings were made using a Multiclamp 700A amplifier (Axons Instruments, Molecular Devices, Sunnyvale, California, USA). Excitatory currents were measured at a holding potential of −70 mV, and action potentials were recorded in cell-attached configuration. Custom software for instrument control and acquisition was written in Matlab (MathWorks, Natick, Massachusetts, USA).

LSPS by glutamate uncaging

We performed LSPS as described previously [3]. Briefly, we added to the external solution (in mM): 0.37 nitroindolinyl (NI)-caged glutamate (Tocris), 0.005 CPP (Tocris), 4 $CaCl_2$ and 4 $MgCl_2$. Focal photolysis of the caged glutamate compound was accomplished with a 1-ms light stimulus consisting of 100 pulses from a pulsed UV laser (wavelength, 355 nm with a repetition rate of 100 kHz; DPSS Lasers, Santa Clara, California USA).

The stimulus grid for LSPS mapping in mouse cortical slices consisted of stimulation of a 16 × 16 grid with 75 μm spacing resulting in a mapping region of 1.125 × 1.125-mm. In rat cortical slices the stimulus grid was 20 × 20 with 75 μm spacing resulting in a mapping region of 1.425 × 1.425-mm. For thalamic uncaging in auditory thalamocortical slices in the mouse the stimulus grid was 16 × 16 with 60 μm spacing (900 × 900-μm mapping region). The pattern of stimulation was designed to avoid revisiting the vicinity of sites recently stimulated (see ref. [3] for details). UV flashes were presented every 1 s. Each trial included a test pulse to measure electrophysiological parameters.

To align the stimulus grid consistently for all cells in horizontal (tonotopic) slices we used two landmarks. We centered the x-axis of the grid on the anterior end of the hippocampus (where the fimbria exits the hippocampus). For the y-axis we aligned the second row of the stimulus grid to the L1/2 border because it is the most prominent layer boundary in the auditory cortex. In the rat auditory cortex, for the y-axis we aligned the third row of the stimulus grid on the L1/2 border, and the x-axis on the border of CA3 and the dentate gyrus.

Although in the main text we refer to low and high frequency areas in the tonotopic slice, we did not assess tonotopy for each preparation, so these are putative labels.

To align the stimulus grid consistently for all cells in coronal (isofrequency) slices we also used two landmarks. We centered the x-axis on the boundary between the dorsal and ventral divisions of the lateral geniculate nucleus. We centered the y-axis in the same way as in the horizontal slices. Due to small variations between slices in the x-axis alignment, we shifted the input maps so that all the somata were aligned to the center of the map in average maps. For each cell we measured the following spatial coordinates: distance from the soma to the pial surface, L1/2 border, and the horizontal center of the map. For thalamic uncaging the stimulating grid was placed to cover the entire MGBv.

To measure how far from the soma a UV flash can evoke an action potential and to calibrate the laser power across cells, we performed cell-attached recordings to detect action potentials (APs) from cells in L4, 5 and 6 to construct excitation profiles (Supplementary Fig. 10). To construct these maps, a smaller stimulus grid was used: for L4 and L6 neurons an 8 × 8 grid with 50 μm spacing. For L5 pyramidal neurons we used an 8 × 16 grid with the same spacing to test for dendritically evoked spiking. From these measurements we found that a 30 mW laser power evoked robust and reliable synaptic responses in the cells patched while maintaining the spatial resolution of the technique (how far from the soma can action potentials be evoked) to less than 100 μm ([2, 5]).

Analysis of LSPS data

To isolate synaptic input responses, the mean current amplitude per stimulus site was calculated in the 50 ms epoch after the direct response time window (7.5 ms after UV stimulus) and expressed as mean charge transfer (pA * synaptic epoch). The values for each stimulus site are represented as pixels in a colormap. For every cell we obtained 2 to 4 maps to create an average input map. These averaged single-cell maps were used for group averages and for all analyses. Interpolated maps are used for illustration purposes only. Given the low correlation of neighboring neurons in A1 we chose to analyze laminar contributions on a single-cell basis to reduce noise. To calculate the contribution of synaptic input from each presynaptic layer on a single-cell basis, we found the pixel with the maximum value and included pixels greater than 50% of this max to calculate the mean. We only included perisomatic pixels that had more than 50% of the cells in the group being analyzed to avoid poor averaging due to direct stimulation sites. We also analyzed presynaptic laminar projections from average population maps (Supplementary Fig. 11) and found similar trends. To find the horizontal distance between the soma and the infragranular sites (pixels) with the strongest excitatory inputs (hot spot), we analyzed the portion of the input maps below L4 (Fig. 4a). We summed the synaptic input along columns and found the column contributing the highest input and included (as part of the hot spot) neighboring columns that were within 1 standard deviation of the summed columnar input (across all columns). The distances reported are to the center of the hotspot. In this analysis we did not include cells with input maps containing multiple hotspots.

Most laminar boundaries were determined for every slice; the markings in each figure represent the averages of the thicknesses measured. The boundary between L1 and L2 is

clear from the almost complete absence of neurons in L1. Layer 2 is the densest layer in A1 and its boundary with L3 was evident upon visual inspection. Further, there were morphological and functional differences between these two layers, which we examined extensively in our study. The boundary between L3 and L4 is poorly defined in the rat and mouse A1. Both layers are populated by pyramidal cells (L4 lacks spiny stellates), both receive thalamic input and in our tracing experiments we found that they both send commissural axons to the contralateral A1. Further, Nissl staining does not produce consistent cell-density differences between these layers[11]. Therefore, we relied on L3 and L4 thicknesses reported in a previous study [11]. The transition from L4 to L5 was clear from the presence of large pyramidal cells in L5. Finally, L5 and L6 differed in the shape and size of their pyramidal cells. All of our laminar boundaries are consistent with a previous study on mouse auditory cortical laminar variation [11].

In vivo recording methods

Surgery: We made a craniotomy (2 mm by 3mm) on the left auditory cortex of anesthetized (30 mg/kg ketamine, 0.24 mg/kg medetomidine) CBA mice aged 28–35 days postnatal to perform cell-attached recordings (10–50 MΩ seal). We targeted neurons in the same area and layers characterized *in vitro* (L2/3 140–300 μm below the cortical surface) using patch electrodes containing the same intracellular solution described above, except that instead of Alexa-594 we used biocytin (1%). *Stimuli*: All recordings were conducted in a double-walled sound booth (Industrial Acoustics Company, Bronx, NY). We used a custom built real-time Linux system (200 kHz sampling rate) driving a high-end Lynx L22 audio card (Lynx Studio Technology Inc., Newport Beach, CA) with an ED1 electrostatic speaker (Tucker-Davis Technologies, Alachua, FL) in free-field configuration (speaker located 8 cm lateral to, and facing, the contralateral ear). The stimuli used were 100 and 500 ms long pure-tones of 16 frequencies logarithmically spaced between 1 to 40 kHz, presented at 5, 20, 50 and 80 dB SPL. All tones were presented in a fixed pseudo-random sequence at a rate of one tone per 2 seconds. We also used 100 ms long white noise stimuli presented at 20, 50 and 80 dB SPL. Based on the timing and tuning properties of the single units and Local Field Potentials (LFPs) at multiple locations we determined that the region mapped was the primary auditory cortex [9]. To further corroborate the location of our *in vivo* recordings and to confirm that the anatomical location of our coronal and horizontal slice recordings were from primary auditory cortex, in some animals we combined LFP recordings with injections of a fluorescent dextran (Supplementary Fig. 12; tetramethylrhodamine 3000 MW, Molecular Probes, Eugene, Oregon, USA). *Histology*: After physiological characterization of each neuron, we performed juxtacellular filling ([17, 18]) and perfused the animals using 4% paraformaldehyde in phosphate buffer. We unambiguously recovered 20 neurons (10 from L2 and 10 from L3). *Analysis*: To quantify any changes in the firing rate during pure tones, we divided the responses into eight 25 ms epochs, which included 50 ms prior to the stimulus and 50 ms post. In the frequency domain, responses were grouped into half octaves. This gave us an 8×8 matrix of responses for each intensity. We subtracted the pre-stimulus spontaneous rate from the corresponding trials and then found the maximum response in the post stimulus period. Finally, we took the average of the maxima for 20, 50 and 80 dB and compared these measurements for L2/3.

DiI retrograde tracing

To determine whether the cortical area mapped in the mouse auditory cortex was primary auditory cortex, we made small injections of DiI (dissolved in xylene to restrict spatial spread of the tracer) in thalamocortical slices. This slice preparation was developed to capture projections from the MGBv to primary auditory cortex [12]. Injected thalamocortical slices (500 μm thick) were incubated for 4–6 weeks at 37 °C (n = 6).

Cholera toxin injections

To characterize the laminar pattern of contralateral projections from the left auditory cortex (the hemisphere where all data was collected) to the right auditory cortex, we injected the retrograde tracer cholera toxin subunit B with Alexa Fluor 488 (Invitrogen, molecular probes, Carlsbad CA, USA). We performed a small craniotomy (1mm by 1mm) over the right auditory cortex under the same anesthesia and protocols described for the *in vivo* recordings. Using a picospritzer (Parker Instrumentation, OH, USA), we injected the tracer at a concentration of 2μg/μL; the injection site spanned all cortical layers. The animals (n = 4) were allowed to recover for 3 days to a week before being perfused.

Statistical analysis

Analysis of significant differences was performed using unpaired *t* tests and one-way ANOVA, with significance defined as $P < 0.05$. All data points are plotted ± the standard error of the mean (s.e.m.) unless otherwise noted.

Supplementary Material

Refer to Web version on PubMed Central for supplementary material.

Acknowledgements

Barry Burbach for invaluable technical help. Siddartha Joshi for invaluable input on juxtacellular labeling. Noah Gray, Gonzalo Otazu, and Troy Hackett for helpful discussions. Wyeth Bair for spike detection software. All LSPS hardware control and data acquisition was performed using ephus (http://www.ephus.org). This work was supported by grants from the NIH, the Patterson Foundation (H.V.O.), the Swartz Foundation, and Autism Speaks.

References

1. Douglas RJ, Martin KA. Neuronal circuits of the neocortex. Annu Rev Neurosci. 2004; 27:419–451. [PubMed: 15217339]
2. Dantzker JL, Callaway EM. Laminar sources of synaptic input to cortical inhibitory interneurons and pyramidal neurons. Nat Neurosci. 2000; 3:701–707. [PubMed: 10862703]
3. Shepherd GM, Svoboda K. Laminar and columnar organization of ascending excitatory projections to layer 2/3 pyramidal neurons in rat barrel cortex. J Neurosci. 2005; 25:5670–5679. [PubMed: 15958733]
4. Callaway EM, Katz LC. Photostimulation using caged glutamate reveals functional circuitry in living brain slices. Proc Natl Acad Sci U S A. 1993; 90:7661–7665. [PubMed: 7689225]
5. Shepherd GM, Pologruto TA, Svoboda K. Circuit analysis of experience-dependent plasticity in the developing rat barrel cortex. Neuron. 2003; 38:277–289. [PubMed: 12718861]
6. Bureau I, von Saint Paul F, Svoboda K. Interdigitated paralemniscal and lemniscal pathways in the mouse barrel cortex. PLoS Biol. 2006; 4:e382. [PubMed: 17121453]

7. Weiler N, Wood L, Yu J, Solla SA, Shepherd GM. Top-down laminar organization of the excitatory network in motor cortex. Nat Neurosci. 2008; 11:360–366. [PubMed: 18246064]
8. Barbour DL, Callaway EM. Excitatory local connections of superficial neurons in rat auditory cortex. J Neurosci. 2008; 28:11174–11185. [PubMed: 18971460]
9. Stiebler I, Neulist R, Fichtel I, Ehret G. The auditory cortex of the house mouse: left-right differences, tonotopic organization and quantitative analysis of frequency representation. J Comp Physiol [A]. 1997; 181:559–571.
10. Read HL, Winer JA, Schreiner CE. Functional architecture of auditory cortex. Curr Opin Neurobiol. 2002; 12:433–440. [PubMed: 12139992]
11. Anderson LA, Christianson GB, Linden JF. Mouse auditory cortex differs from visual and somatosensory cortices in the laminar distribution of cytochrome oxidase and acetylcholinesterase. Brain Res. 2009; 1252:130–142. [PubMed: 19061871]
12. Cruikshank SJ, Rose HJ, Metherate R. Auditory thalamocortical synaptic transmission in vitro. J Neurophysiol. 2002; 87:361–384. [PubMed: 11784756]
13. Kimura A, Donishi T, Sakoda T, Hazama M, Tamai Y. Auditory thalamic nuclei projections to the temporal cortex in the rat. Neuroscience. 2003; 117:1003–1016. [PubMed: 12654352]
14. Linden JF, Liu RC, Sahani M, Schreiner CE, Merzenich MM. Spectrotemporal structure of receptive fields in areas AI and AAF of mouse auditory cortex. J Neurophysiol. 2003; 90:2660–2675. [PubMed: 12815016]
15. Lefort S, Tomm C, Floyd Sarria JC, Petersen CC. The excitatory neuronal network of the C2 barrel column in mouse primary somatosensory cortex. Neuron. 2009; 61:301–316. [PubMed: 19186171]
16. DeWeese MR, Wehr M, Zador AM. Binary spiking in auditory cortex. J Neurosci. 2003; 23:7940–7949. [PubMed: 12944525]
17. Pinault D. A novel single-cell staining procedure performed in vivo under electrophysiological control: morpho-functional features of juxtacellularly labeled thalamic cells and other central neurons with biocytin or Neurobiotin. J Neurosci Methods. 1996; 65:113–136. [PubMed: 8740589]
18. Joshi S, Hawken MJ. Loose-patch-juxtacellular recording in vivo-a method for functional characterization and labeling of neurons in macaque V1. J Neurosci Methods. 2006; 156:37–49. [PubMed: 16540174]
19. Velenovsky DS, Cetas JS, Price RO, Sinex DG, McMullen NT. Functional subregions in primary auditory cortex defined by thalamocortical terminal arbors: an electrophysiological and anterograde labeling study. J Neurosci. 2003; 23:308–316. [PubMed: 12514229]
20. Matsubara JA, Phillips DP. Intracortical connections and their physiological correlates in the primary auditory cortex (AI) of the cat. J Comp Neurol. 1988; 268:38–48. [PubMed: 3346383]
21. Imig TJ, Brugge JF. Sources and terminations of callosal axons related to binaural and frequency maps in primary auditory cortex of the cat. J Comp Neurol. 1978; 182:637–660. [PubMed: 721972]
22. Games KD, Winer JA. Layer V in rat auditory cortex: projections to the inferior colliculus and contralateral cortex. Hear Res. 1988; 34:1–25. [PubMed: 3403382]
23. Lima SQ, Hromadka T, Znamenskiy P, Zador AM. PINP: a new method of tagging neuronal populations for identification during in vivo electrophysiological recording. PLoS One. 2009; 4:e6099. [PubMed: 19584920]
24. Smith PH, Populin LC. Fundamental differences between the thalamocortical recipient layers of the cat auditory and visual cortices. J Comp Neurol. 2001; 436:508–519. [PubMed: 11447593]
25. Hubel DH, Wiesel TN. Receptive fields, binocular interaction and functional architecture in the cat's visual cortex. J Physiol. 1962; 160:106–154. [PubMed: 14449617]
26. Armstrong-James M, Fox K, Das-Gupta A. Flow of excitation within rat barrel cortex on striking a single vibrissa. J Neurophysiol. 1992; 68:1345–1358. [PubMed: 1432088]
27. Van Hooser SD, Heimel JA, Chung S, Nelson SB, Toth LJ. Orientation selectivity without orientation maps in visual cortex of a highly visual mammal. J Neurosci. 2005; 25:19–28. [PubMed: 15634763]

28. Van Hooser SD, Heimel JA, Chung S, Nelson SB. Lack of patchy horizontal connectivity in primary visual cortex of a mammal without orientation maps. J Neurosci. 2006; 26:7680–7692. [PubMed: 16855096]
29. Ohki K, Chung S, Ch'ng YH, Kara P, Reid RC. Functional imaging with cellular resolution reveals precise micro-architecture in visual cortex. Nature. 2005; 433:597–603. [PubMed: 15660108]
30. Koulakov AA, Chklovskii DB. Orientation preference patterns in mammalian visual cortex: a wire length minimization approach. Neuron. 2001; 29:519–527. [PubMed: 11239440]
31. Yoshimura Y, Dantzker JL, Callaway EM. Excitatory cortical neurons form fine-scale functional networks. Nature. 2005; 433:868–873. [PubMed: 15729343]
32. Bandyopadhyay S, Shamma SA, Kanold PO. Dichotomy of functional organization in the mouse auditory cortex. Nat Neurosci. 2010; 13:361–368. [PubMed: 20118924]
33. Rothschild G, Nelken I, Mizrahi A. Functional organization and population dynamics in the mouse primary auditory cortex. Nat Neurosci. 2010; 13:353–360. [PubMed: 20118927]
34. Hromadka T, Deweese MR, Zador AM. Sparse representation of sounds in the unanesthetized auditory cortex. PLoS Biol. 2008; 6:e16. [PubMed: 18232737]
35. Chechik G, et al. Reduction of information redundancy in the ascending auditory pathway. Neuron. 2006; 51:359–368. [PubMed: 16880130]
36. Nelken I. Processing of complex sounds in the auditory system. Curr Opin Neurobiol. 2008; 18:413–417. [PubMed: 18805485]
37. Bar-Yosef O, Rotman Y, Nelken I. Responses of neurons in cat primary auditory cortex to bird chirps: effects of temporal and spectral context. J Neurosci. 2002; 22:8619–8632. [PubMed: 12351736]
38. Kowalski N, Versnel H, Shamma SA. Comparison of responses in the anterior and primary auditory fields of the ferret cortex. J Neurophysiol. 1995; 73:1513–1523. [PubMed: 7643163]
39. Kaur S, Rose HJ, Lazar R, Liang K, Metherate R. Spectral integration in primary auditory cortex: laminar processing of afferent input, in vivo and in vitro. Neuroscience. 2005; 134:1033–1045. [PubMed: 15979241]
40. Metherate R, et al. Spectral integration in auditory cortex: mechanisms and modulation. Hear Res. 2005; 206:146–158. [PubMed: 16081005]
41. Ts'o DY, Gilbert CD, Wiesel TN. Relationships between horizontal interactions and functional architecture in cat striate cortex as revealed by cross-correlation analysis. J Neurosci. 1986; 6:1160–1170. [PubMed: 3701413]
42. Rockland KS, Lund JS. Widespread periodic intrinsic connections in the tree shrew visual cortex. Science. 1982; 215:1532–1534. [PubMed: 7063863]
43. Boyden ES, Zhang F, Bamberg E, Nagel G, Deisseroth K. Millisecond-timescale, genetically targeted optical control of neural activity. Nat Neurosci. 2005; 8:1263–1268. [PubMed: 16116447]

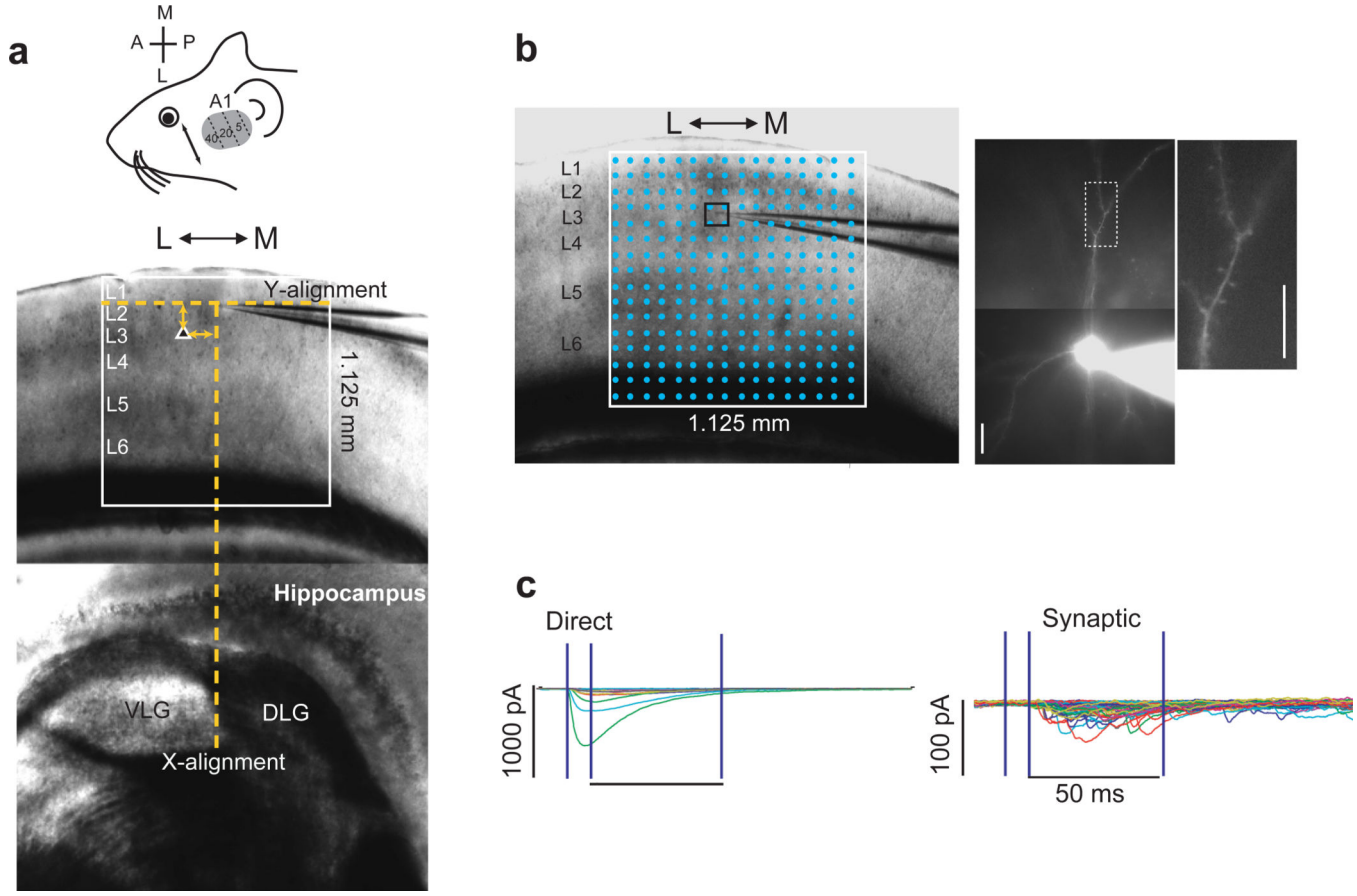

Figure 1. Auditory cortex LSPS experimental preparation

(**a**) Coronal brain slice (cut along the lateral (L) medial (M) axis) containing the primary auditory cortex and underlying subcortical area used for studying the organization along the isofrequency axis. The *white box* outlines the stimulus grid, and the *dashed lines* represent the landmarks used to align the grid from animal to animal. For each cell we measured the distance of the soma from the L1/2 border and the middle of the grid. (The ventral and dorsal divisions of the lateral geniculate nucleus (VLG and DLG, respectively) are labeled as landmarks). **(b)** (*left*) Stimulus grid showing the 16×16 points of uncaging. (*right*) Picture of a patched cell filled with Alexa and magnification of a dendritic branch (scale bar is 15 μm). (**c**) (*left*) Examples of *direct responses*, *i.e.* those evoked by the direct activation of receptors by uncaged glutamate in the neuron under study. (*right*) Examples of *synaptic responses*, i.e. EPSCs elicited by triggering action potentials in neurons presynaptic to the neuron under study. The vertical lines through the traces mark the time window to detect direct responses (first 2 vertical lines) and synaptic events (second and third vertical lines).

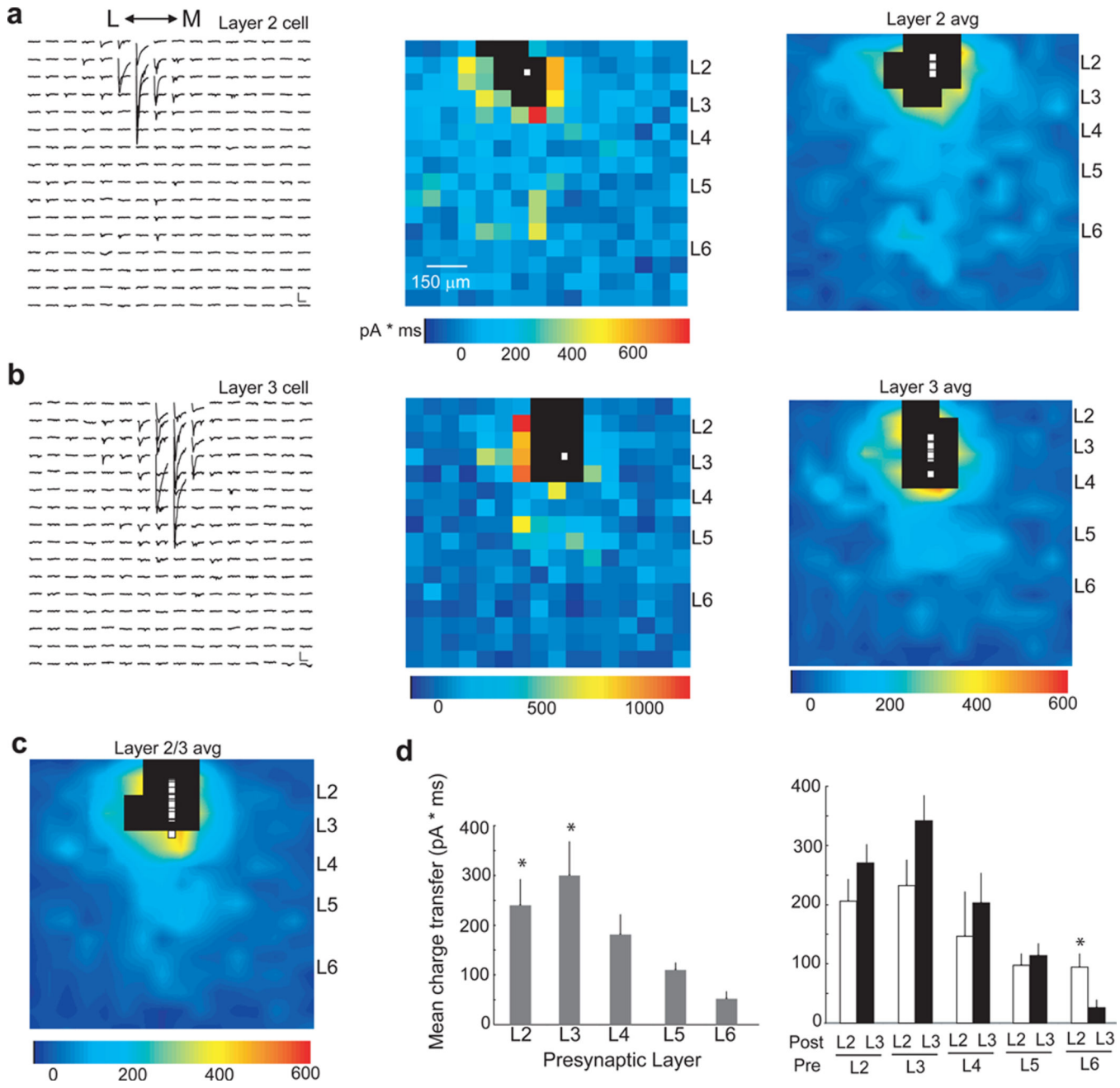

Figure 2. Synaptic input organization along the isofrequency axis

(**a**) (*left*) Map of synaptic traces used to generate the colormap (*middle*) of a L2 neuron. Each trace on the left (and the corresponding pixel on the right) represents to a point on the uncaging grid (see Figure 1**b**). Pixels contaminated with a direct response are shown in black; for all other pixels, the color indicates the charge transferred during the EPSC integration window defined in Fig. 1**c**. The white square indicates the location of the soma. (*right*) Interpolated average input map for all L2 neurons recorded (n = 11). Maps were re-aligned to place the somata on the center of the x-axis of the map. (**b**) Single-cell trace map (*left*) and colormap (*middle*), and interpolated population map (*right*) of all L3 neurons

recorded (n = 15). (**c**) Interpolated map of all L2/3 neurons combined (n = 26). (**d**) Mean laminar input (n = 26) to L2/3 neurons (*left*). Local connections (within L2/3) provided the majority of the input (asterisks; $P << 0.01$ ANOVA). (*right*) Summary of the mean laminar input to L2 and L3 arising from all cortical layers. Asterisks indicate laminar input where the difference in synaptic input between L2 and L3 was significantly different ($P < 0.05$, n = 26, t-test). Data are presented as mean ± s.e.m. Scale bars in synaptic traces are 50 pA and 100 ms.

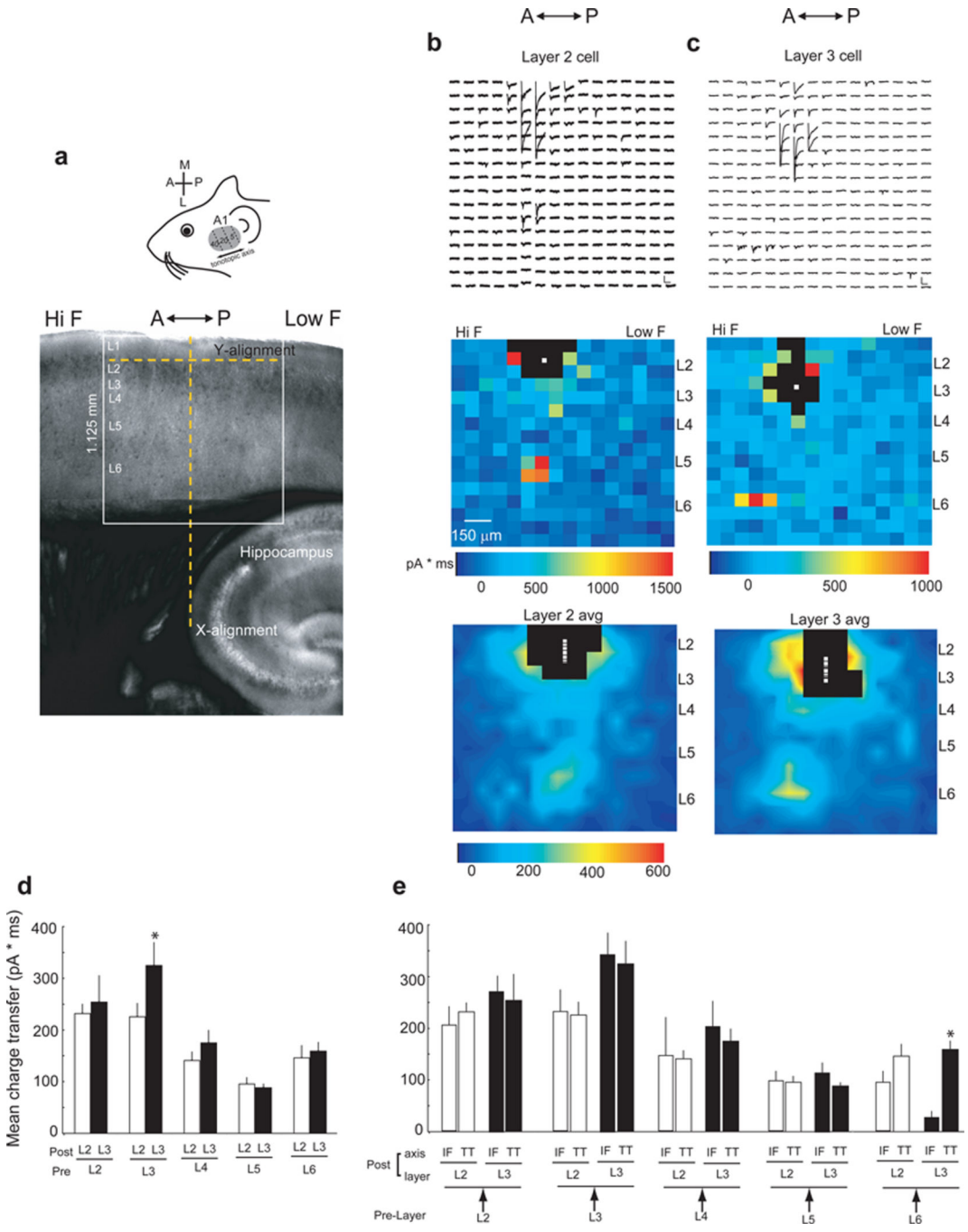

Figure 3. Synaptic input organization along the tonotopic axis

(**a**) Horizontal slices used to capture the anterior-posterior (A↔P) representation of tonotopy in auditory cortex. Image of a horizontal slice depicting the anatomical landmarks used to align the stimulation grid (*white box*). The anterior (left) side of the slice corresponds to the putative high frequency (Hi F) portion of A1 and the posterior (right) side to putative low frequencies (Low F). (**b**) Trace map of synaptic input map to a L2 neuron (*top*) and its colormap (*middle*). Interpolated population map of all L2 neurons recorded (*bottom*, n = 15). (**c**) Single-cell trace map (*top*) and colormap (*middle*), and interpolated population map

(*bottom*) of all L3 neurons recorded (n = 15). (**d**) Summary of the mean laminar input to L2 and L3 arising from all cortical layers. Asterisk indicates laminar input where the difference in synaptic input between L2 and L3 was significantly different ($P < 0.05$, n = 30, t-test). (**e**) Grand summary and comparison of the mean laminar input to L2/3 along the isofrequency (IF) and tonotopic (TT) axes. Asterisk indicates laminar input where the difference in synaptic input between the tonotopic and isofrequency axes was significantly different ($P << 0.01$, t-test). Data are presented as mean ± s.e.m. Scale bars in synaptic traces are 50 pA and 100 ms.

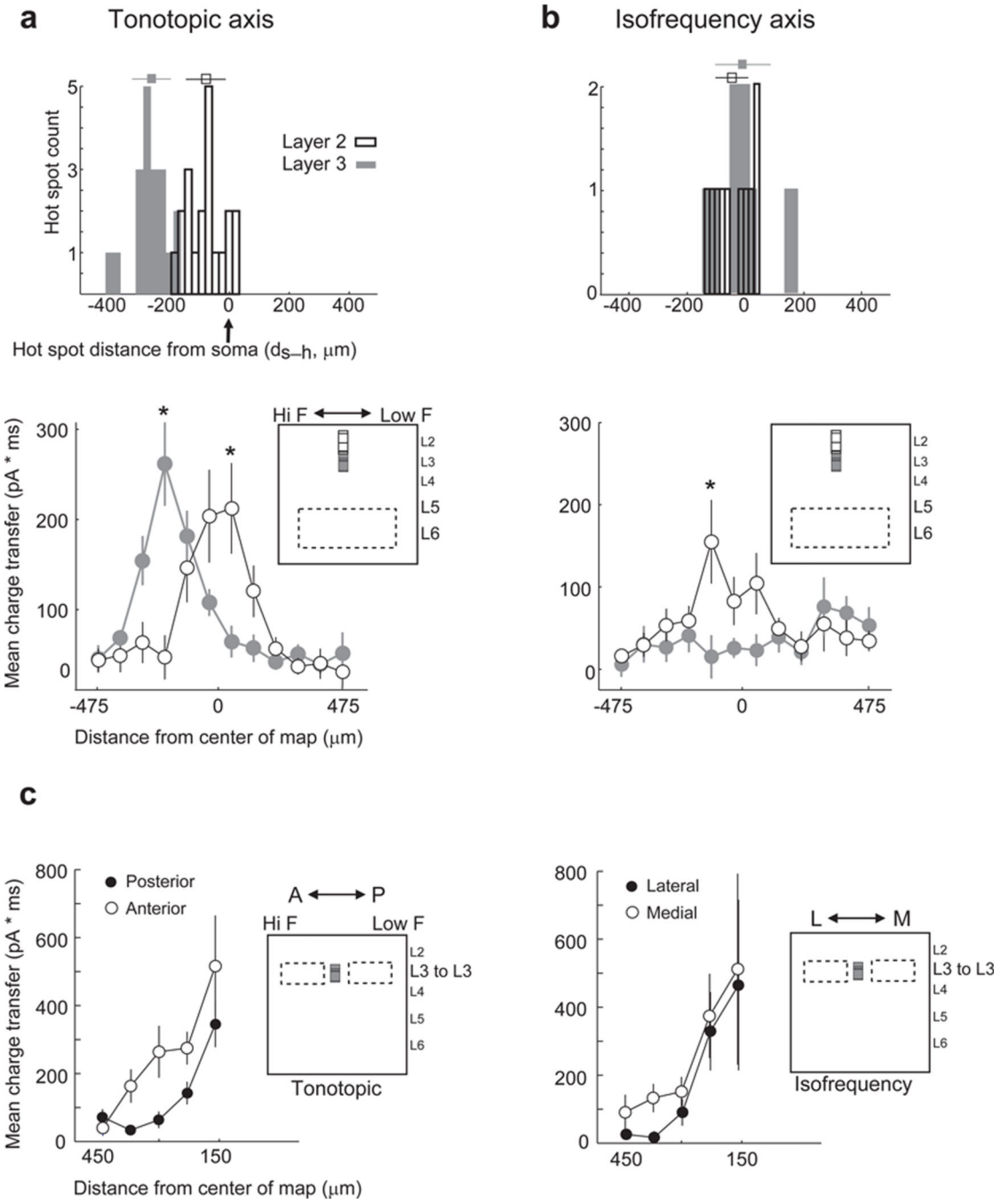

Figure 4. Along tonotopic but not isofrequency axis, inputs to L3 arise asymmetrically out –of-column

(**a–b**): L5/6 input to L3, but not L2, arose out-of-column preferentially from putative high-frequency neurons in tonotopic slices. *Top* panels show the distribution of the horizontal distances between the soma and its hotspot (d_{s-h}) of presynaptic input along the tonotopic (n = 39) and isofrequency (n = 22) axes for each L2 and L3 neuron. The square points show the mean (± s.e.m) of the L2 and L3 distributions. *Bottom* panels show columnar average of L5/6 input. Asterisks indicate columns where input to L2 was significantly different from

L3. The insets show the uncaging grid and the relative position of the cortical area where inputs were averaged (dashed rectangle). (**c**) Local L3 input to L3 arose preferentially from putative high-frequency neurons in tonotopic slices. Relative contribution of local input (within L3) arising from the anterior and posterior (putative higher and lower frequency, respectively) input sites of the L3 cells mapped in the tonotopic slice. The plots show the mean charge transfer along columns. Input arising from the higher frequency sites was greater than from lower frequency sites in the tonotopic slice (*left*), but not the isofrequency (*right*). Inputs arising from posterior and medial sites were reflected on the x-axis for display purposes. Insets show the uncaging grid and the relative position of the cortical area where inputs were averaged (dashed rectangles to the left and right of L3 somata). Data are presented as mean ± s.e.m.

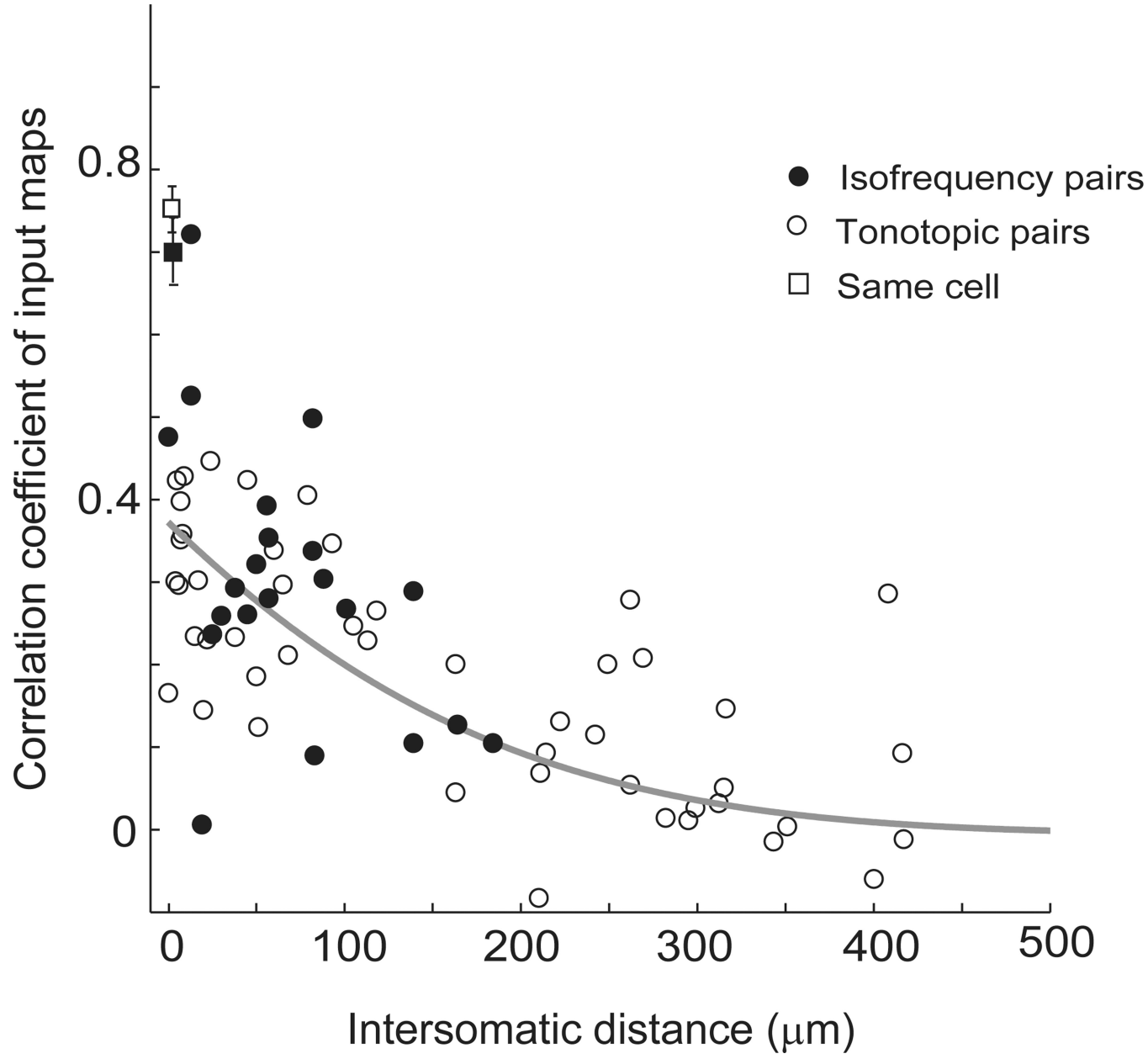

Figure 5. Synaptic input correlation between pairs of auditory cortical neurons

Plot shows the relationship between the correlations of input maps in pairs of cells in the same slice as a function of their intersomatic horizontal distance. We compared population correlation along the tonotopic and isofrequency axes. The gray line is the exponential fit (*0.37 * exp(−x/159)*). Square points showing the correlation of maps obtained for the same cell represent the theoretical upper limit of correlation given the experimental variability.

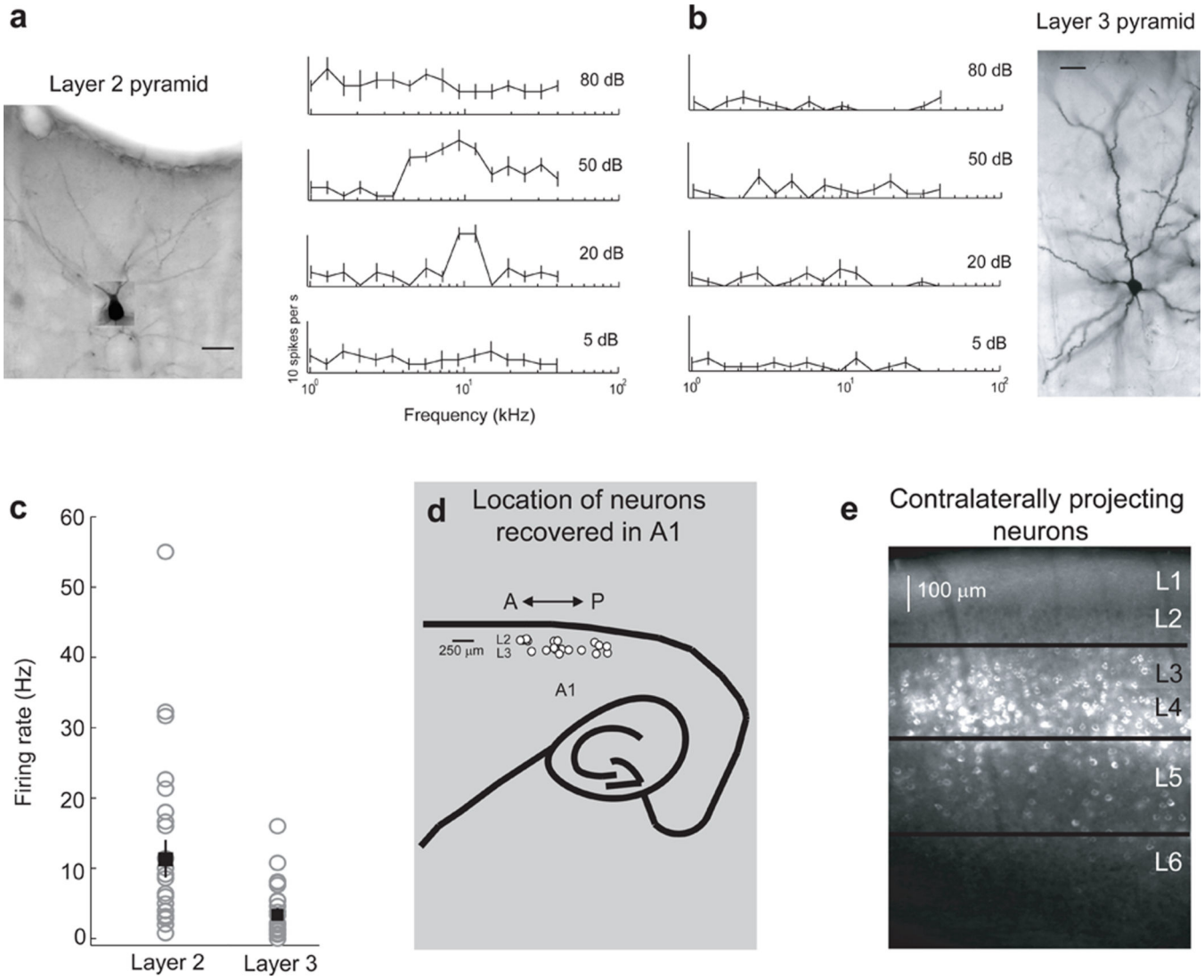

Figure 6. L3 neurons are less responsive to simple auditory stimuli than L2 neurons

(**a**) Frequency-response plot (*right*) for a L2 neuron (*left*) assessed using cell-attached recording. (**b**) Frequency-response plot (*left*) for a L3 neuron (*right*) assessed using cell-attached recording. Scale bars in **a** and **b** are 25 µm. (**c**) Summary of the differences in evoked firing rate between the L2 and L3 neurons recovered (n = 20). For each intensity, we found the octave bin with the maximum firing rate in the 150 ms post-stimulus epoch; we then averaged over the maximum for intensities 20, 50, and 80. The difference in firing rates was insensitive to outliers (e.g. removing the three highest firing rates from each group increased significance from $P < 10^{-4}$ to $P < 10^{-5}$, n = 20, t-test). (**d**) Location of neurons characterized in ***c***. (**e**) Labeling in the left auditory cortex after injection of a retrograde tracer (cholera toxin) into the right auditory cortex shows that L3 but not L2 neurons project to the contralateral auditory cortex. Data are presented as mean ± s.e.m.